

Optical-digital joint design method for Cassegrain optical system with large *FOV**

SUN Lin and CUI Qingfeng**

School of Opto-Electronic Engineering, Changchun University of Science and Technology, Changchun 130022, China

(Received 22 April 2022; Revised 23 June 2022)

©Tianjin University of Technology 2022

The field of view (*FOV*) of the traditional Cassegrain optical system is small, generally only 0.1° — 0.2° . In order to enlarge the *FOV*, it is usually necessary to add correction groups or change the mirror type, but it introduces color difference and complicates the structure. In this study, an optical digital joint design method is put forward to expand the *FOV* of the Cassegrain optical system. First, the structural parameters of the system are optimized to control the aberration. Then, based on the wavefront aberration theory, the wavefront aberration model is constructed using Zernike polynomials, and the point spread function model is established using Fourier transform. Finally, the image is processed using the spatial transform deconvolution algorithm. The *FOV* of the Cassegrain optical system is expanded using only primary and secondary mirror structures. The simulation experiment of the Cassegrain optical system shows that the *FOV* is expanded approximately 6 times, and the imaging quality is improved. The simulation results indicate that our method is feasible.

Document code: A **Article ID:** 1673-1905(2022)09-0525-5

DOI <https://doi.org/10.1007/s11801-022-2068-8>

The Cassegrain optical system is a typical reflective optical system. It has the advantages of no chromatic aberration, compact structure, and good imaging in the paraxial field of view (*FOV*). It is widely used in aviation, aerospace, and other long-distance detection fields^[1,2]. Further, it has no axial aberration. However, its off-axis aberration is serious, narrowing the *FOV* to generally no more than 0.2° . At present, there are three main methods to expand the *FOV* of Cassegrain optical system, preposition correction method, postposition correction method, and changing the reflector type. The Schmidt-Cassegrain structure is widely used in the preposition correction method, but the diameter of the pre correction plate is too large to be processed^[3,4]. Postposition correction method usually added refractive lens group behind the primary mirror and secondary mirror, to correct the out-of-axis aberration^[5,6]. The last method is to change the surface type of the primary and secondary mirrors, such as Ritchey-Chretien optical system, Dall-Kirkham system, etc^[7]. However, the above methods make the optical system more complex, increase the difficulty of thermalization, introduce color difference, and limit the working wave band. In recent years, a new imaging method of computational imaging has emerged^[8,9]. Scholars combine optical design with computational imaging to overcome the limitations of traditional imaging systems, such as improving the diffraction efficiency of diffractive op-

tical system^[10], expanding the *FOV* of off-axis optical system^[11], proposing optical-digital joint design method for near eye display^[12].

In this paper, an optical-digital joint design method is proposed to realize a large *FOV* imaging of the Cassegrain optical system. First, we analyzed the aberration distribution of Cassegrain system, and obtained the variation law of the aberration in the whole *FOV*. Then we construct the wavefront aberration model through the aberration distribution. Then, the point spread function (PSF) model is obtained by Fourier transform. Finally, the spatial variation deconvolution algorithm is used to accurately process the aberration, improve the low image quality caused by the aberration of the large *FOV*, and achieve the purpose of expanding the *FOV*. A typical Cassegrain optical system is simulated, and the simulation results that the modulation transfer function (MTF) of each *FOV* and the imaging quality are significantly improved. The *FOV* of the Cassegrain optical system is expanded without adding a correction lens group or changing the surface shape.

The imaging principle of the optical system is as follows

$$g(x, y) = PSF(x, y) \otimes f(x, y) + \eta(x, y), \quad (1)$$

where $g(x, y)$ represents the image, \otimes represents convolution operation, $f(x, y)$ represents the object, and $\eta(x,$

* This work has been supported by the National Science and Technology Major Project of China (No.51-H34D01-8358-13/16).

** E-mail: qfcui163@163.com

y) represents noise. Through Eq.(1), we can find that the reason for the decline of the imaging quality of the optical system is the $PSF(x, y)$. $PSF(x, y)$ contains aberration information. When we know $g(x, y)$ and $PSF(x, y)$, we can get $f(x, y)$.

No chromatic aberration exists in the reflective optical system. However, monochromatic aberration is observed in the Cassegrain optical system.

While estimating the curvature, blocking ratio, and magnification of the primary and secondary mirrors of the Cassegrain optical system, the main aberrations, such as spherical aberration, coma, and astigmatism, affect the imaging quality. In the optical design process, we can optimize the conic coefficients of the primary and secondary mirrors to obtain a front-end optical system with a large coma. This optimization can accelerate the model construction speed, reduce the construction difficulty, reduce the ringing effect, and improve the effect and speed of post-processing.

First, we construct the wavefront aberration model of the optical system. Wavefront aberration includes the aberration information of optical system. The wavefront aberration can express as

$$W(x, y) = \sum_{i=1}^9 a_i Z_i + \sum_{j=10}^{\infty} a_j Z_j, \quad (2)$$

where a_i represents the different Zernike coefficients, and $\sum_{j=10}^{\infty} a_j Z_j$ represents the term which can compensate for wavefront aberration. For general optical systems, the first 9 Zernike terms generally represent primary aberrations, and the higher-order terms represent advanced aberrations. Because we only considered the influence of coma, only Zernike items 1, 4 and 8 are used.

Considering that the Cassegrain optical system has a coaxial symmetry, the wavefront aberration $W_y(x, y)$ in a single FOV direction (such as Y direction) can be first obtained. Then the wavefront aberration in the whole FOV can be estimated through rotation. In this way, the Zernike item in the X FOV direction can be ignored to

reduce the workload and increase the construction speed.

The construction method is shown in the following formula:

$$\begin{cases} \mathbf{A}_i(hy) = [a_i(0), a_i(m), a_i(2m), \dots, a_i(1)]^T \\ \mathbf{Z}_i = [Z_1, Z_2, Z_3, \dots, Z_i]^T \\ \mathbf{W}_y = [\mathbf{A}_1, \mathbf{A}_2, \mathbf{A}_3, \dots, \mathbf{A}_i] \times \mathbf{Z}_i \\ \mathbf{W}(x, y) = \text{Rotate}\{\mathbf{A}_y, \theta\} \end{cases}, \quad (3)$$

where hy is the coordinate of normalized Y FOV , m is the sampling step of normalized Y FOV , θ is the angle between the line from the sampling point to the center of the image plane and the Y -axis, and Rotate is to rotate the matrix by θ degree around the center point.

Next, we construct the generalized pupil function based on the wavefront aberration as

$$\mathbf{P}(x, y) = p(x, y) \exp[ik\mathbf{W}(x, y)], \quad (4)$$

where $k=2\pi/\lambda$ is the wave number and $\mathbf{P}(x, y)$ is the geometric pupil function. $\mathbf{W}(x, y)$ obtained from Eq.(3) is substituted into Eq.(4) to obtain the system generalized pupil function $\mathbf{P}(x, y)$. Then, $\mathbf{P}(x, y)$ is Fourier transformed, and PSF is obtained by squaring the modulus of the transformation result as

$$PSF(x, y) = |\mathcal{F}\{\mathbf{P}(x, y)\}|^2, \quad (5)$$

where \mathcal{F} represents Fourier transform. Finally, according to the constructed PSF model, the spatial change-constrained least-squares restoration algorithm is used to calculate the optimal solution. This algorithm employs the alternating direction method of multipliers to complete the image restoration^[13,14] as

$$\arg \min \left\{ \left\| PSF(x, y) * \hat{f} - g(x, y) \right\|_2^2 + \gamma \left\| \nabla^2 \hat{f} \right\|_p \right\}, \quad (6)$$

where argmin represents the function for finding minimum value, γ represents the weights of terms for suppressing noise and ringing, ∇^2 represents the Laplace operator, p represents the different norm types, and \hat{f} represents the approximate solution of the object.

The flow chart of the method is displayed in Fig.1.

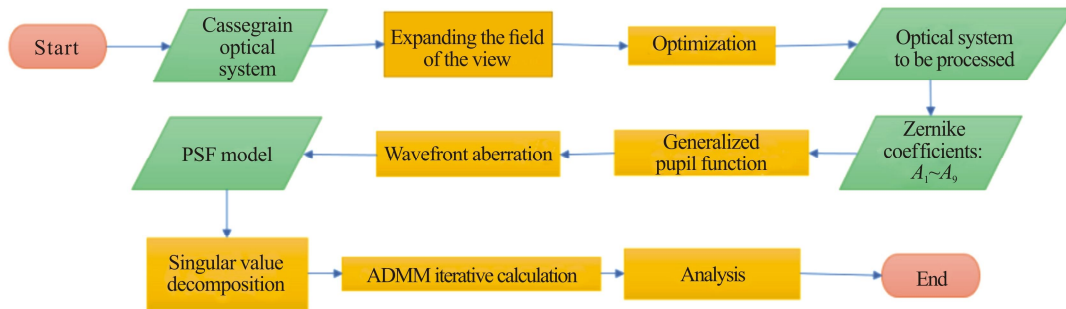


Fig.1 Flow chart of the proposed method

In addition, we simulated a classical Cassegrain optical system, and the designed optical system indexes are listed in Tab.1.

In the design process, the conic coefficients of the primary and secondary mirrors are set as variables, and the front-end optical system with large coma is obtained

through iterative optimization. The optical system structure is shown in Fig.2.

Tab.1 Optical system parameters

Parameter	Value
Focal distance	550 mm
$F/\#$	4
Wavelength	900—1 700 nm
FOV	0.2°
Expected FOV	1.2°

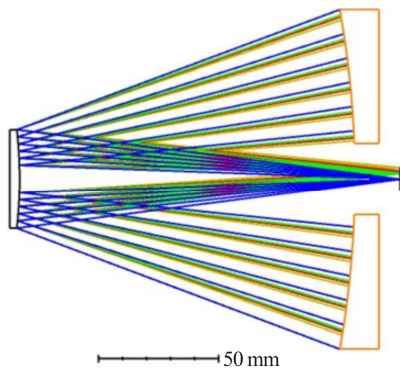


Fig.2 Optical system diagram

The structural parameters of the optical system are shown in Tab.2.

Tab.2 Structural parameters of the optical system

	Primary mirror	Secondary mirror
Radius (mm)	-393.18	-176.67
Thickness (mm)	139.83	158.80
Semi-diameter (mm)	74.79	20.59
Surface type	Paraboloid	Hyperboloid
Conic	-1	-4.463

According to the method mentioned above, we can observe the functional relationship between the first and eighth terms of Zernike polynomials, as shown in Fig.3.

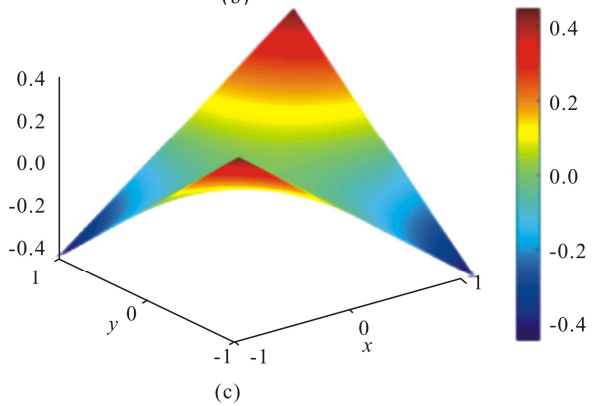
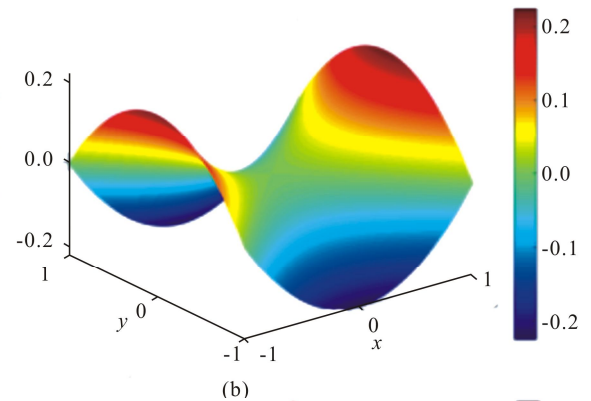
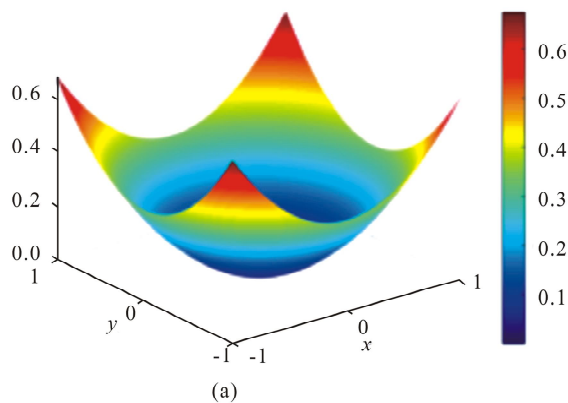
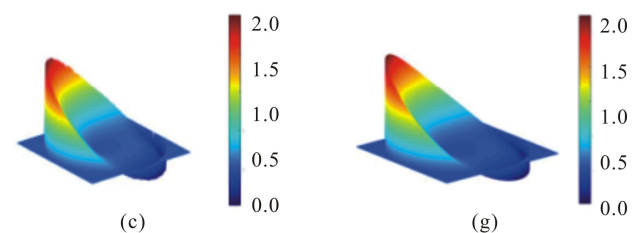
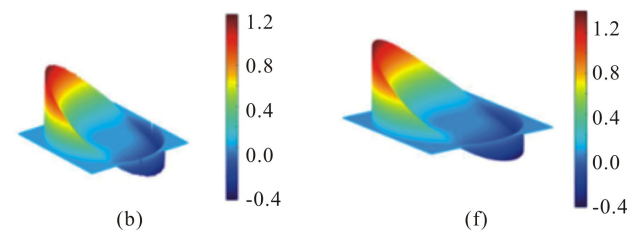
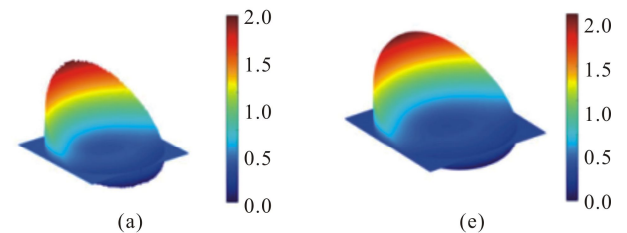


Fig.3 Fitting surface graphs of Zernike coefficients ($X \in [-1, 1], Y \in [-1, 1]$): (a) Coefficient Z_1 ; (b) Coefficient Z_4 ; (c) Coefficient Z_8

Next, substituting the surface equation in Fig.3 into Eq.(3), we can get the $W(x, y)$ of optical system. In order to verify the accuracy of the constructed model, we compared it with the wavefront aberration diagram in the optical design software, as shown in Fig.4.



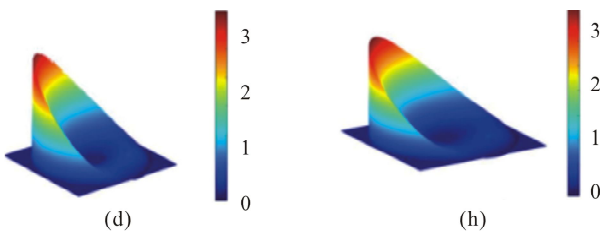


Fig.4 Wavefront aberration comparison of Cassegrain optical system at different FOVs in optical design software: (a) 0°, (b) 0.3°, (c) 0.42°, and (d) 0.6°; Corresponding diagrams of the constructed model: (e) 0°, (f) 0.3°, (g) 0.42°, and (h) 0.6°

Then, we substitute the obtained wavefront aberration model into Eq.(4) to obtain the generalized pupil function. Subsequently, the PSF model of the optical system is obtained by substituting $P(x, y)$ into Eq.(5). Similarly, we select three FOV points to verify the accuracy of the model.

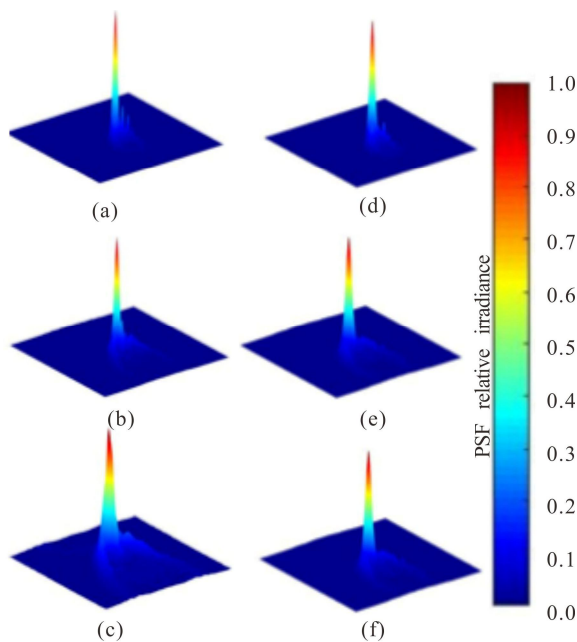


Fig.5 PSF comparison of Cassegrain optical system: (a) PSF of ZEMAX at 0.3° FOV; (b) PSF of ZEMAX at 0.42° FOV; (c) PSF of ZEMAX at 0.6° FOV; (d) PSF of model at 0.3° FOV; (e) PSF of model at 0.42° FOV; (f) PSF of model at 0.6° FOV

Finally, we combine the PSF model and the algorithm of Eq.(6) to simulate the imaging simulation diagram of the optical system. The comparison of the results before and after processing is shown in Figs.6 and 7.

The original Fig.6 was photographed by the author, and Fig.6(a) was obtained through optical system simulation imaging. Fig.6(b) was obtained after restoration.

Fig.7 shows the simulation of the intercepting part of ISO 12233 Resolution Board, and the resolution is significantly improved after restoration. MTF is a common

index to evaluate imaging quality. Therefore, in Fig.7, we select 4 regions to measure MTF according to the FOV distribution. We use the Slanted-Edge method to measure MTF, and the results are shown in Fig.8^[15,16]. It can be seen that MTF has significantly improved after recovery.

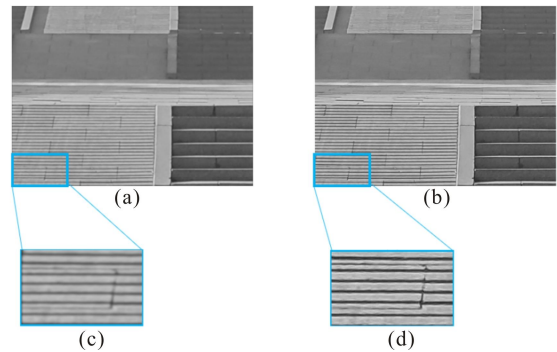


Fig.6 Comparison before and after algorithmic processing: (a) Blurred image simulated by the clear image passing through the optical system; (b) Restoration image; (c) Detail enlarged view of the selected area in (a); (d) Detail enlarged view of the selected area in (b)

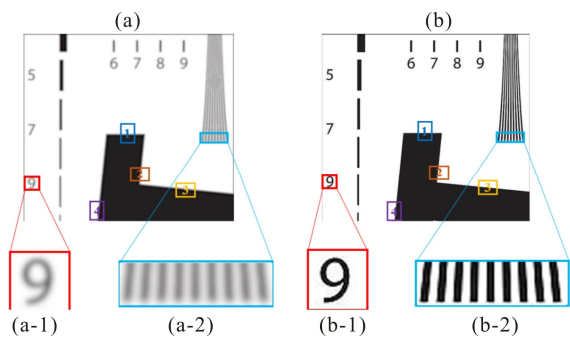
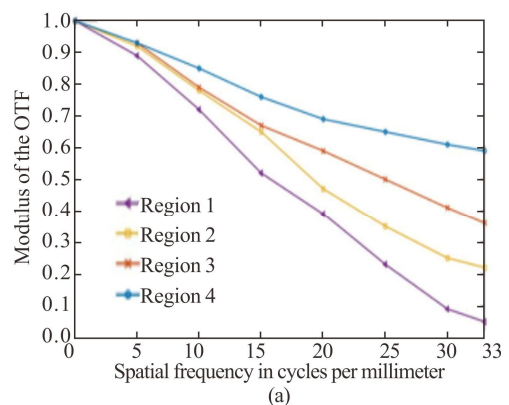


Fig.7 Part of ISO12233 Resolution Board simulation results: (a) Blurred image simulated by the clear image passing through the optical system, (a-1) and (a-2) are the detail enlarged views of the selected areas in (a); (b) Image processed by algorithm, (b-1) and (b-2) are the detail enlarged views of the selected areas in (b)



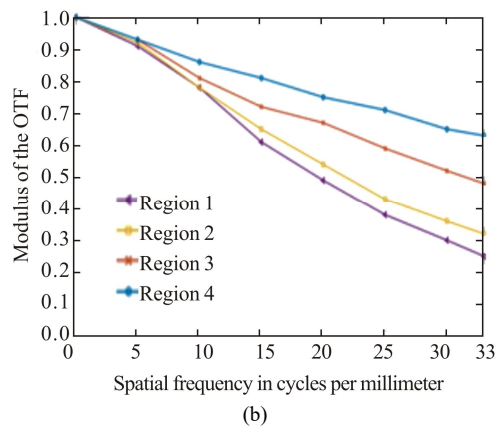


Fig.8 MTF curves of the optical system: (a) Areas 1—4 in Fig.7(a); (b) Areas 1—4 in Fig.7(b)

In conclusion, we proposed an optical digital joint design method, which can effectively expand the *FOV* of a Cassegrain optical system. First, we design the front-end optical system by analyzing the aberration distribution of Cassegrain optical system. Then we build the PSF model with the aberration information. Finally, combined with the spatial variation deconvolution algorithm, the image quality degradation of Cassegrain optical system caused by the aberration at large *FOV* is eliminated. The simulation results of a typical Cassegrain optical system show that the processed image quality has been significantly improved, the *FOV* is expanded by 6 times, and the MTF has been significantly improved. The *FOV* of the Cassegrain optical system is expanded without adding a correction lens group or changing the reflector type.

Statements and Declarations

The authors declare that there are no conflicts of interest related to this article.

References

- [1] ZHOU M F, YANG H J, JIANG P, et al. Structure design of a conic lens pair for improving the transmission efficiency of a Cassegrain antenna[J]. *Applied optics*, 2019, 58(13): 3410-3417.
- [2] MA D L. Recommended conceptual optical system design for China's large optical-infrared telescope (LOT)[J]. *Optics express*, 2018, 26(1): 108-119.
- [3] BRYCHIKHIN M N, CHKHALO N I, EIKHORN Y O, et al. Reflective Schmidt-Cassegrain system for large-aperture telescopes[J]. *Applied optics*, 2016, 55(16): 4430-4435.
- [4] FISCHER R E, TADIC G B. *Optical system design*[M]. 2nd ed. New York: MCGRAW HILL, 2008: 138-142.
- [5] ROCHA M C, GONCHAROV A V. Aplanatic meniscus lens corrector for Ritchey-Chrétien telescopes[J]. *Optics express*, 2022, 30(4): 6076-6089.
- [6] ZHANG J G, NIE Y F, FU Q, et al. Optical-digital joint design of refractive telescope using chromatic priors[J]. *Chinese optics letters*, 2019, 17(5): 052201.
- [7] SMITH W J. *Modern optical engineering*[M]. 4th ed. New York: MCGRAW HILL, 2008: 472-512.
- [8] KUNDUR D, HATZINAKOS D. Blind image deconvolution[J]. *IEEE signal processing magazine*, 1996, 13(3): 43-64.
- [9] JUN K, TATIANA A, FIGEN S, et al. Computational optical sensing and imaging 2021: introduction to the feature issue[J]. *Applied optics*, 2022, 61(9): COSI1-COSI4.
- [10] HU Y, CUI Q F, ZHAO L D, et al. PSF model for diffractive optical elements with improved imaging performance in dual-waveband infrared systems[J]. *Optics express*, 2018, 26(21): 26845-26857.
- [11] SUN L, CUI Q F, ZONG Z, et al. A method to increase the field of view of an imaging optical system[J]. *IEEE photonics journal*, 2022, 14(1): 1-10.
- [12] SUN L, CUI Q F. Optical-digital integrated design method for near-eye display imaging system[J]. *IEEE access*, 2022, 10: 50314-50322.
- [13] SROUBEK F, KAMENICKY J, LU Y M. Decomposition of space-variant blur in image deconvolution[J]. *IEEE signal processing letters*, 2016, 23(3): 346-350.
- [14] KOPRIVA I. Single-frame multichannel blind deconvolution by nonnegative matrix factorization with sparseness constraints[J]. *Optics letters*, 2005, 30(23): 3135-3137.
- [15] MASAOKA K, YAMASHITA T, NISHIDA Y, et al. Modified slanted-edge method and multidirectional modulation transfer function estimation[J]. *Optics express*, 2014, 22(5): 6040-6046.
- [16] XIE X F, FAN H D, WANG A D, et al. Error of the slanted edge method for measuring the modulation transfer function of imaging systems[J]. *Applied optics*, 2018, 57(7): B83-B91.